ELM suppression through density profile modification with lithium wall coatings in the National Spherical Torus Experiment

R. Maingi[a], T.H. Osborne[b], B.P. LeBlanc[c], R.E. Bell[c], J. Manickam[c], P.B. Snyder[b], J.E. Menard[c], D.K. Mansfield[c], H.W. Kugel[c], R. Kaita[c], S.P. Gerhardt[c], S.A. Sabbagh[d], and the NSTX research team

[a]*Oak Ridge National Laboratory, Oak Ridge TN, 37831 USA*

[b] *General Atomics, San Diego CA, USA*

[c]*Princeton Plasma Physics Laboratory, PO Box 451, Princeton, NJ, 08543 USA*

[d]*Columbia University, New York, NY USA*

Abstract

Reduction or elimination of edge localized modes (ELMs) while maintaining high confinement is essential for future fusion devices, e.g. the International Thermonuclear Experimental Reactor which has been designed for H-mode operation. An ELM-free regime was recently obtained in the National Spherical Torus Experiment, following the application of lithium onto the graphite plasma facing components. Edge stability calculations indicate that the pre-lithium discharges were unstable to peeling/ballooning modes with toroidal mode number (n) in the range $2<n<5$. ELM pre-cursors in this n-range were identified in fast magnetics data from those discharges. Following the application of lithium, the edge pressure profile broadened substantially, mainly from a shift of the edge density profile due to reduced recycling. The lithium-enhanced discharges are calculated to be far from the edge stability boundaries, because of the broader pedestal profiles. These discharges exhibit an improvement in normalized energy confinement time of up to 50%, with no sign of ELMs up to the global stability limit.

Body Text

Periodic ejections of particles and power from the edge of fusion research devices have been observed since the discovery of the high confinement or H-mode[1]. These instabilities are termed edge localized modes (ELMs), and they have been observed in nearly all toroidal confinement devices operating in H-mode with sufficient heating power to reach the instability threshold[2]. The onset of large ("Type 1") ELMs has been correlated with measured plasma profiles exceeding an operational window on the edge plasma pressure gradient and edge current, imposed by the ideal magnetohydrodynamic (MHD) stability of coupled peeling and ballooning modes[3, 4]. Calculations of these ideal MHD limits for future devices, such as the International Thermonuclear Experimental Reactor, indicate that ELMs are to be expected there also. While ELMs purge the edge plasma of impurities and enable a quasi-steady operation in present day devices, they also deliver a pulsed power load that would limit the lifetime of plasma-facing components (PFCs) unless the energy release of each individual ELM was made sufficiently small. Thus control of ELM size and elimination of ELMs altogether has received high priority in international fusion research. While the quiescent H-mode (QH-mode)[5] and use of external resonant magnetic perturbations (RMP)[6] are attractive regimes with suppressed ELMs, the former scenario is thought to require substantial velocity shear, and the latter is thought to require internal coils close to the plasma, both of which present challenges in future devices.

As in other fusion research devices, ELMs are routinely observed[7] in nearly all H-mode discharges in the National Spherical Torus Experiment (NSTX)[8]. H-mode access is facilitated in spherical tokamaks (ST) with fueling from the high-field side[9, 10]; however,

the difficulty in installing a fully controllable valve in the center stack coupled with the good particle confinement in STs leads to a secular density rise even in most ELMy H-mode scenarios in both the NSTX[11] and the Mega-Amp Spherical Tokamak[12]. Density control in DIII-D H-mode discharges has been demonstrated with strong in-vessel pumping[13]; in this case, optimal pumping is obtained for particular shapes in which the outer divertor strike point is placed near the pump plenum opening. An alternative being tested in NSTX is lithium evaporation onto large portions of the divertor PFCs, which in principle could provide density control for a wider variety of boundary shapes while enhancing the energy confinement[14]. In recent experiments in NSTX, sufficiently thick lithium coatings also resulted in complete ELM suppression[15-18]. The goal of this paper it to present evidence that the density/pressure profile changes correlated with lithium wall coatings are responsible for the ELM suppression.

In the remainder of this paper, we 1) document the change in discharge characteristics and kinetic profiles in pre- and post-lithium discharges; 2) show that the ELM suppression corresponds to stabilization of low-n peeling/ballooning modes based on stability calculations using equilibria constructed from those kinetic profiles; and 3) identify low-n magnetic fluctuation ELM pre-cursors in the range predicted for the pre-lithium stability calculations, where n is toroidal mode number. The final post-lithium, enhanced confinement discharges avoid the edge stability limit, but reach the global stability limit with a fraction of the input power of the pre-lithium discharges. We note that while these post-lithium ELM-free discharges can suffer from impurity accumulation and secular radiation increase[19], 3-d magnetic perturbations have been shown to

reproducibly trigger ELMs, maintain good confinement, and prevent the impurity buildup[20].

Lithium is introduced into the NSTX vacuum vessel between plasma discharges using a pair of overhead evaporators; no inter-discharge helium glow discharge cleaning was used in this set of experiments[17, 18]. With a high lithium evaporation rate and/or coating thickness, the energy confinement increased such that the heating power needed to be reduced to avoid the global stability limit. The effect of thick lithium wall coatings on discharge characteristics is shown for three discharges (black: pre-lithium, red: post-lithium, low power, blue: post-lithium, intermediate power) in Figure 1. Panel 1b shows a step in neutral beam injected power from 2 to 3 MW at 0.45 sec in the post-lithium discharges; the post-lithium discharge with 4 MW of neutral beam injected power (NBI) disrupted shortly after I_p flat-top (not shown). The post-lithium discharges showed reduced early density and dN/dt, although the eventual density in the lowest power discharge reached the same value as the reference discharge, partly because of the lack of ELMs (panel 1c). Panel 1d shows that the stored energy for the 2 MW post-lithium discharge was comparable to the 4 MW pre-lithium discharge, and that the energy confinement time normalized by the ITER-97 L-mode global scaling[21] was 50% higher in the post-lithium discharges (panel 1e).. Following the 2 MW-3 MW step at 0.45 sec, a global MHD instability terminated the high performance phase (blue curve panel 1d). The The radiated power was comparable out to 0.48 sec in these discharges, despite higher input in the pre-lithium discharge, i.e. the radiated power fraction increased during the ELM-free H-mode phase (panel 1f). Finally the divertor D_α emission was

substantially lower in the post-lithium discharges, indicating reduced recycling, and all signatures of ELM activity vanished (panel 1g).

The dramatic effect of lithium conditioning on the plasma kinetic profiles for the 2 MW (post-lithium) and 4 MW (pre-lithium) discharges from Figure 1 is displayed in Figure 2. The time slice at t=0.415 sec is displayed because the plasma – outer wall gap was nearly identical, and electron density and temperature (n_e, T_e) data from the Thomson Scattering diagnostic and ion temperature and toroidal rotation (T_i, v_{tor}) data from the charge-exchange recombination spectroscopy (ChERS) diagnostic were centered about the same time window to within 1 msec. In the pre-lithium discharge, the T_e gradient increased outside of R=1.42 m, indicating that R=1.42m was the top of the H-mode pedestal (panel 2a). While the T_e gradient outside of R=1.42m was unaffected in the post-lithium discharge, the region of reduced gradient from R=1.36m-1.42m was eliminated; effectively shifting the entire profile upward. In contrast, the entire post-lithium n_e profile appears to be shifted inward by about 2 cm, despite having the same plasma-wall gap (panel 2b). The density inside of R=1.35m was also reduced. The edge and core post-lithium T_i values were increased (panel 2c), while the v_{tor} was higher (lower) in the edge (core) of the post-lithium discharge (panel 2d). Note that the reduction of core n_e and v_{tor} in the post-lithium discharge is consistent with reduced NBI particle fueling and torque input.

To assess the effect of these profile changes on edge stability, an analysis procedure developed for high aspect ratio tokamaks was performed[22, 23]. The procedure is summarized here:

1. Generate magnetics-only equilibria at the time slices of the Thomson Scattering laser pulses using the EFITD code[24].
2. Map the individual n_e, T_e, T_i profiles to normalized poloidal magnetic flux, ψ_N, to construct a single profile from the multiple time slice data. For the pre-lithium ELMy discharge, profile data from the last 20% of the ELM cycle is binned[22], with a maximum time window of 100 msec to minimize the effect of the density ramp in Figure 2. For the post-lithium discharge, multiple profiles using data from 100-200 msec time windows are generated to determine the dependence of the edge stability on density/collisionality.
3. Perform a free boundary kinetic equilibrium fit, using the profiles from step 2 as the target pressure profiles. The target edge current is computed from the neoclassical bootstrap current[25] with Z_{eff} computed from the carbon content as computed from the ChERS data. The stability of these individual equilibria is evaluated with the PEST ideal MHD code[26].
4. Perform a set of fixed boundary kinetic equilibrium fits, while varying the edge pressure gradient at fixed edge current and vice-versa. The stability of these various equilibria is evaluated with the ELITE ideal MHD code[3, 4] to assess the proximity to the peeling mode (high edge current) and ballooning mode (high pressure gradient) boundaries.

A comparison of the plasma total pressure profile and its radial gradient from representative free boundary kinetic eqilibria for the pre- and post-lithium discharges is shown in Figure 3. Note that a different pre-lithium discharge (#129015, programmed identically to #129019) was chosen for this analysis, because three Thomson profiles

were obtained in a 100 msec window in the last 20% of the inter-ELM period. The pre-lithium discharge had a steep pressure gradient very near the separatrix (ψ_N =1), whereas the peak gradient was shifted inward substantially for the post-lithium discharge (panels 3a, 3b), owing primarily to the change in the n_e profile. In addition the spatial width of the steep gradient region is larger in the post-lithium discharge, which also enhanced the edge stability.

PEST calculations of the pre-Lithium discharge equilibria indicate instability to low-n (n=2, 3, 4) peeling/ballooning modes, with the growth rate peaking for n=3. The maximum linear growth rate was computed at 1.5% of the Alfven frequency. The radial displacement from the n=3 mode peaks on the low field side, indicative of the ballooning character of this low-n mode (panel 3c). In comparison, the post-lithium profiles are stable to these modes, because of the increased width of the steep gradient region of the pressure profile.

The fixed boundary kinetic EFITs from step 4 above were shown to be close to the peeling mode instability threshold from ELITE calculations. Figure 4 shows an edge stability space diagram of normalized edge current as a function of normalized pressure gradient[27]. The colors represent contours of the ratio of the mode linear growth rate γ to the diamagnetic drift frequency, ω_*. Here the white rectangle and error bars, representing the experimental profiles and their uncertainties, lie very close to the kink/peeling mode stability boundary. This boundary is the transition from the blue to the red region, which corresponds with $\gamma/\omega_* > 5\%$. While this is an alternate stability threshold criterion than used for assessment with PEST as discussed above, this stability criterion takes into account that rapid diamagnetic drift can stabilize peeling/ballooning modes[23]. The most

unstable mode from ELITE had n=4, i.e. relatively low-n in agreement with the PEST calculation.

The prediction that low-n modes are the most unstable for the pre-lithium discharges is in good agreement with analysis of the NSTX fast magnetics data for ELM pre-cursors (Figure 5), as also seen in other devices[2, 28]. The time dependence of the divertor D_α emission and the Thomson laser timing are shown in panel 5a; note the three Thomson time slices with blue stars from 0.317-0.417 sec that occur within the last 20% of the inter-ELM period. The magnetics data for the ELM near t=0.382 sec shows a growing pre-cursor oscillation in the 50 kHz range, along with the simulated signal (panel 5b black and blue curves). The toroidal phase fit for that precursor shows an n=3 structure in panel 5c. Panel 5d shows the mode number and frequency of all of the ELM pre-cursors with good fits between 0.31 sec and 0.42 sec. It can be seen that the experimental mode number ranges from n=2 to n=5, with a general increase as the density and collisionality ramped during the discharge. The mode frequency varied between 40 and 60 kHz with no clear time dependence.

To summarize, lithium wall coatings suppressed ELMs in otherwise ELMy NSTX discharges, owing ostensibly to recycling and core fueling reduction. The plasma profiles changed substantially as a result, with the n_e profile shifting radially inward by several cm. Thus, the width of the steep pressure gradient increased, which helps to stabilize low-n instabilities. Specifically the pre-lithium (post-lithium) profiles are unstable (stable) to n=2-4 peeling/ballooning modes, based on calculations from two different codes. That these were low-n instabilities is supported by observations of pre-cursor oscillations in the fast magnetics data, which were present in the pre-lithium discharges and absent in

post-lithium discharges, consistent with the physics postulated to be responsible for ELM suppression.

The discharges enabled by the lithium conditioning become ELM-free with a substantial improvement in energy confinement time relative to scalings. Consequently the discharges achieve normalized beta β_N of 5.5, where $\beta_N = aB_t\beta,/I_p$, a = minor radius, B_t = vacuum toroidal magnetic field on axis, β = ratio of plasma stored energy (W_{MHD}) to toroidal magnetic field stored energy ($B_t^2/2\mu_0$), μ_0 = permeability of free space, and I_p = plasma current. The global instability that terminated the high performance phase in Figure 1 had characteristic signatures of a resistive wall mode, indicating that the discharge was operating between the 'no-wall' and 'ideal-wall' β limits in NSTX[29]. In other words, the lithium-enhanced discharges reached global stability limits before reaching edge/ELM stability limits, thereby avoiding large pulsed power loads to the target. Looking ahead, quantitative understanding of the effect of the lithium wall coatings on the density profile remains an area of active research for projection of the effects of lithium in other devices, and research on optimization of triggered ELM scenarios is continuing[20].

This research was supported by the U. S. Dept. of Energy under contracts DE-AC05-00OR22725, DE-AC02-76CH03073, and DE-FC02-04ER54698. We gratefully acknowledge the contribution of the NSTX technical staff and neutral beam operations staff.

Figure Captions

1. Comparison of pre-lithium ELMy discharge (black), and two post-lithium discharges with different NBI power (blue, red): (a) plasma current I_p, (b) neutral beam injected power P_{NBI}, (c) line-average density from Thomson Scattering n_e^{TS}, (d) stored energy from equilibrium reconstruction W_{MHD}, (e) confinement time relative to ITER97L scaling, (f) total radiated power P_{rad}, and (g) divertor D_α emission.
2. Profiles for T_e, n_e, T_i and v_{tor} for pre- and post-lithum discharges (black, red respectively).
3. (a) Kinetic pressure and (b) pressure gradient in normalized flux space for the pre- and post-lithium time slices mentioned above (red and green respectively); (c) poloidal projection of radial displacement for n=3 mode in pre-lithium discharge.
4. Stability boundary from ELITE code with fixed boundary kinetic EFITs for pre-lithium discharge. The experimental data point and uncertainties are given by the white rectangle and error bars, and the peeling mode boundary is shown by the transition region between blue and red.
5. Low-n pre-cursor activity in pre-lithium discharge: (a) D_α emission and timing of Thomson scattering laser pulses, (b) mode growth data (black) and simulation (blue) for ELM pre-cursor near t=0.382 sec, (c) toroidal mode number fit for same ELM showing n=3 mode, and (d) mode number and frequency fits for several ELMs vs. time.

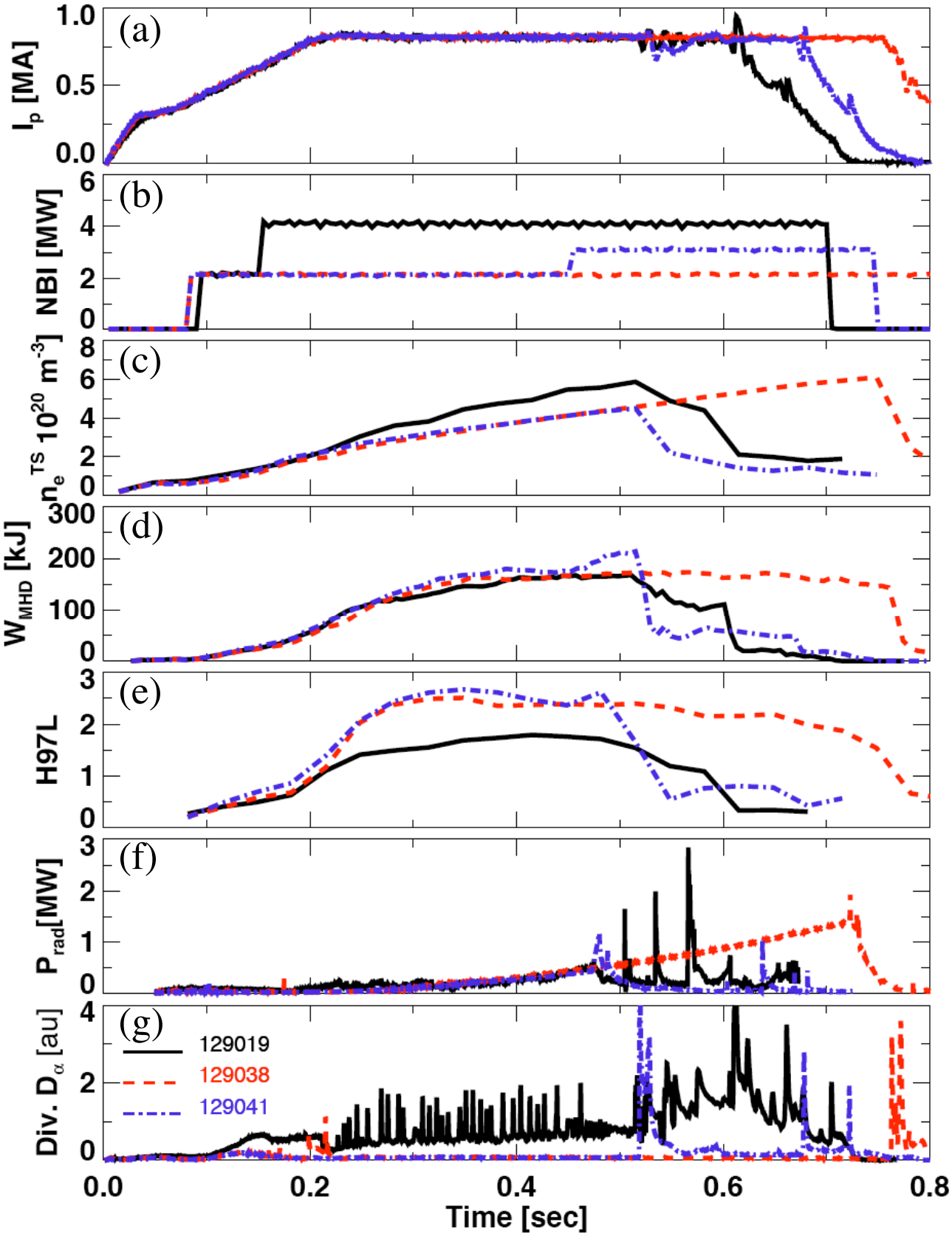
(a)
I_p [MA]
1.0
0.5
0.0
(b)
NBI [MW]
6
4
2
0
(c)
n_e^{TS} 10^{20} m^{-3}]
8
6
4
2
0
(d)
W_{MHD} [kJ]
300
200
100
0
(e)
H97L
3
2
1
0
(f)
P_{rad}[MW]
3
2
1
0
(g)
Div. D_α [au]
4
2
0
129019
129038
129041
0.0
0.2
0.4
0.6
0.8
Time [sec]

Figure 1

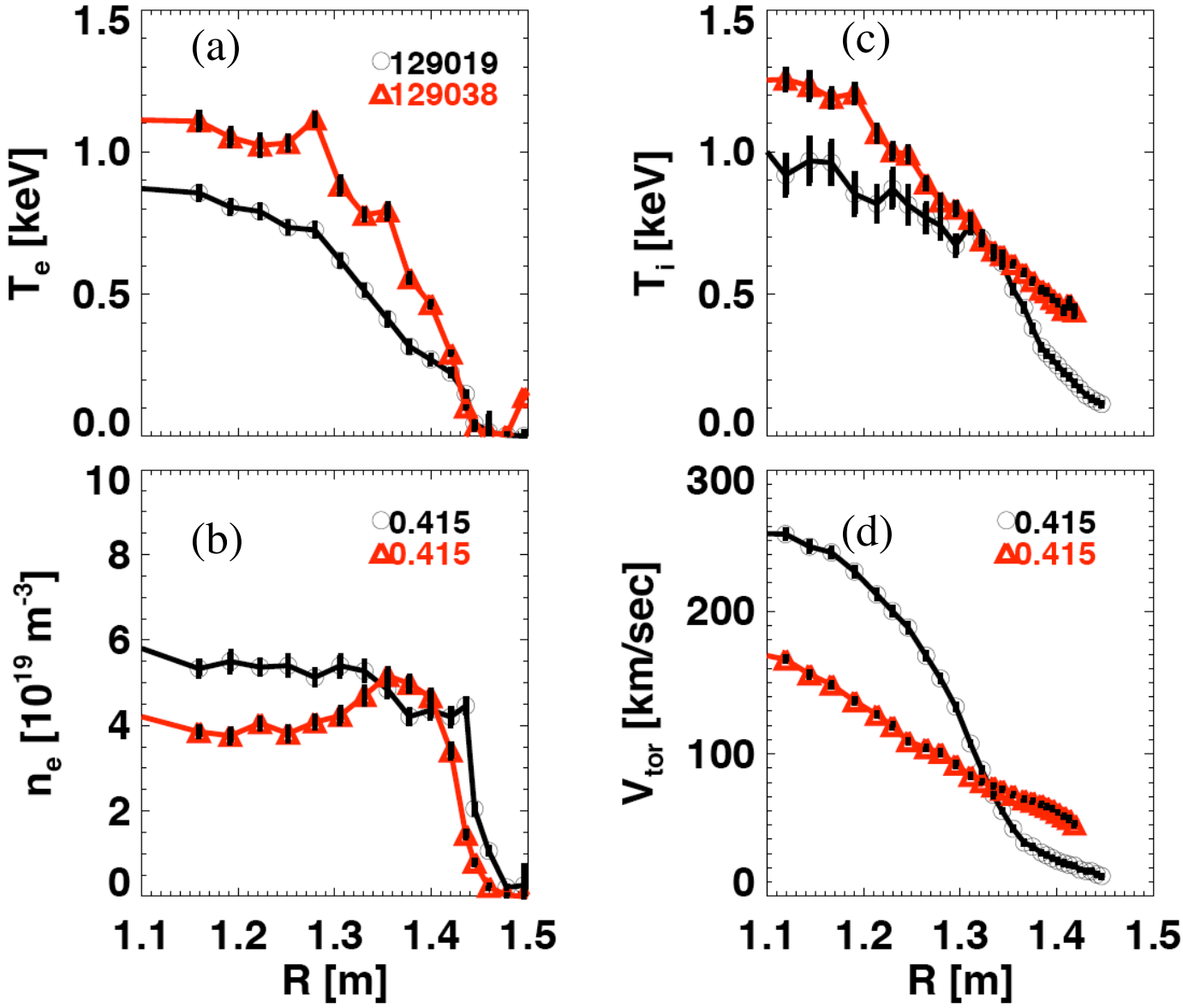
(a)
129019
Δ129038
T_e [keV]
1.5
1.0
0.5
0.0
(c)
T_i [keV]
(b)
0.415
Δ0.415
n_e [10^{19} m^{-3}]
10
8
6
4
2
0
(d)
V_{tor} [km/sec]
300
200
100
1.1
1.2
1.3
1.4
1.5
R [m]

Figure 2

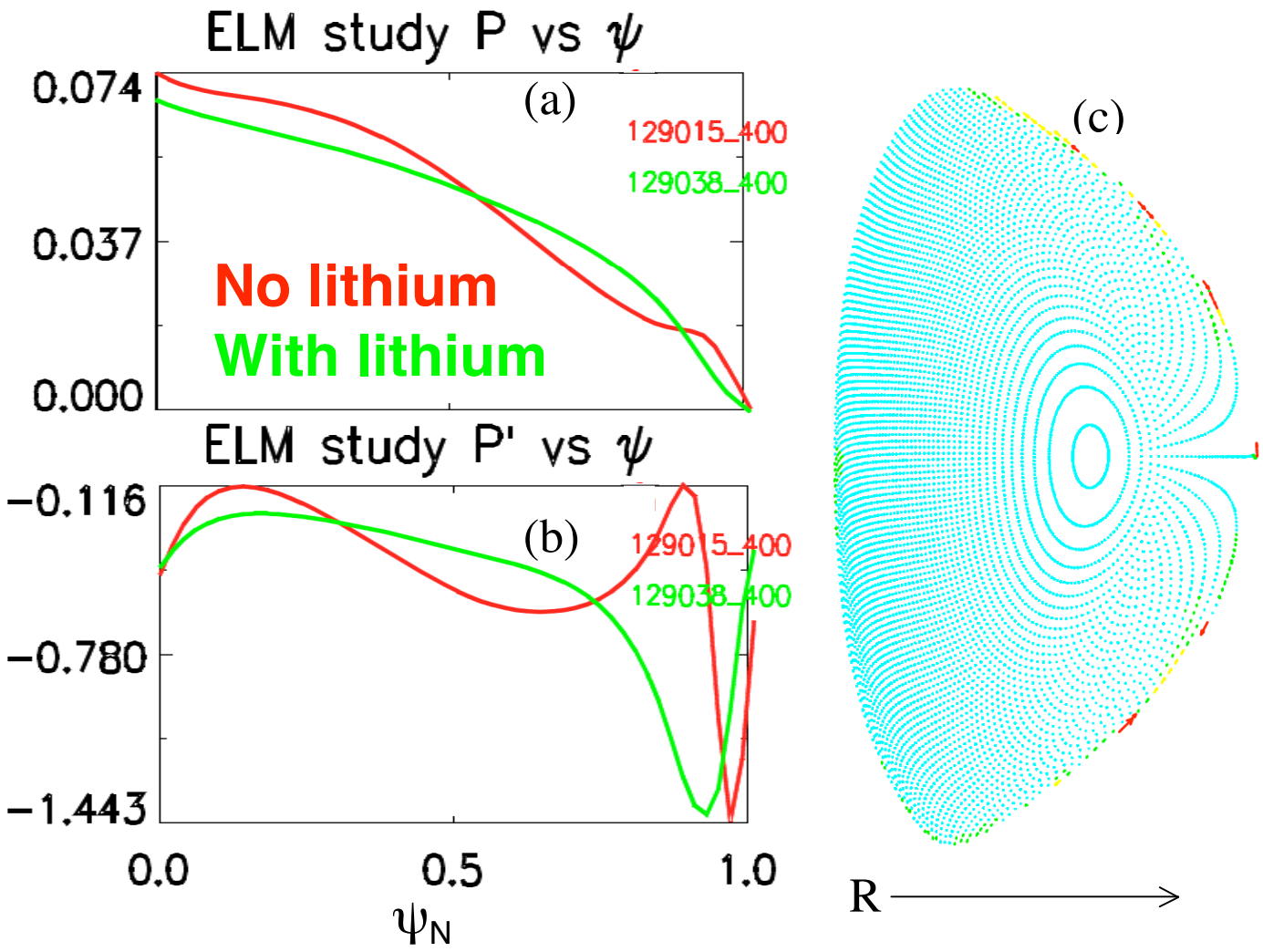
ELM study P vs ψ
0.074
0.037
0.000
(a)
129015_400
129038_400
No lithium
With lithium
ELM study P' vs ψ
−0.116
−0.780
−1.443
(b)
129015_400
129038_400
0.0
0.5
1.0
ψN
(c)
R

Figure 3

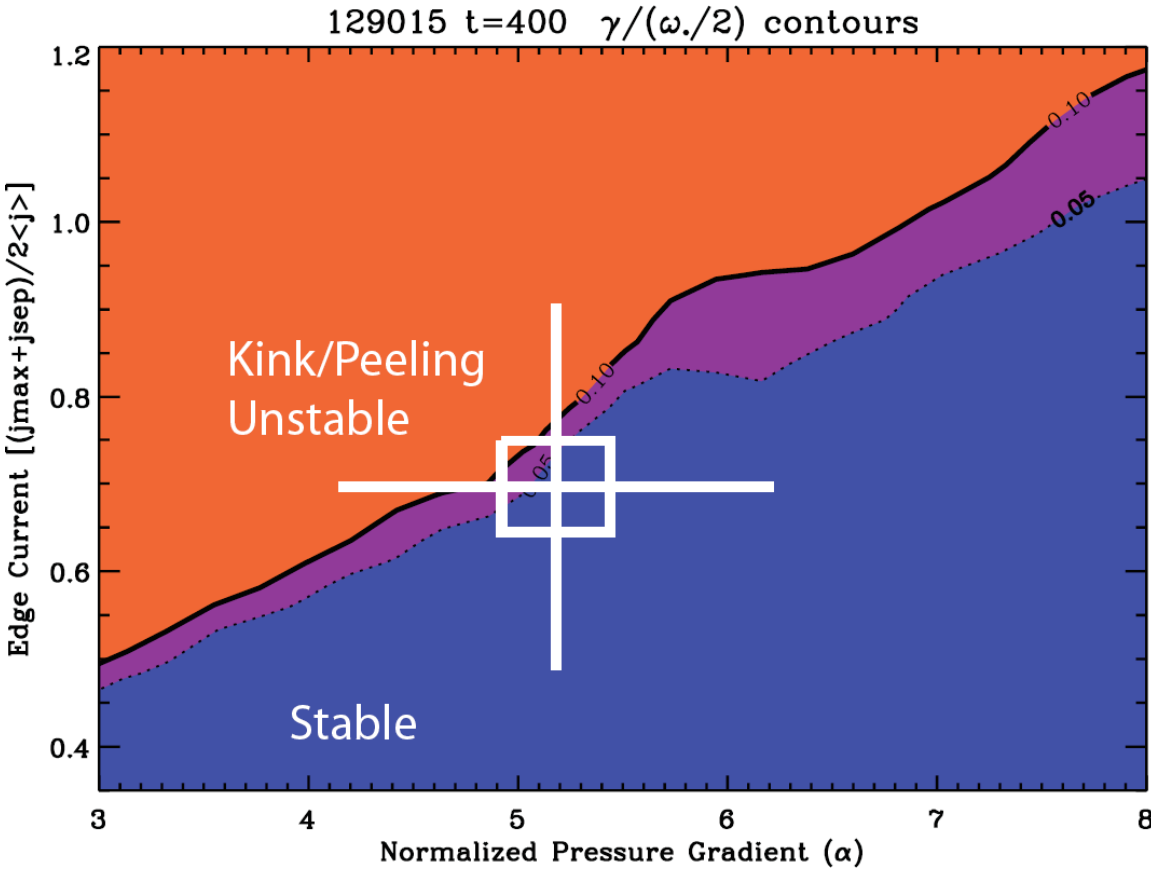
129015 t=400 γ/(ω./2) contours
Kink/Peeling
Unstable
Stable
0.10
0.05
Edge Current [(jmax+jsep)/2<j>]
Normalized Pressure Gradient (α)
1.2
1.0
0.8
0.6
0.4
3
4
5
6
7
8

Figure 4

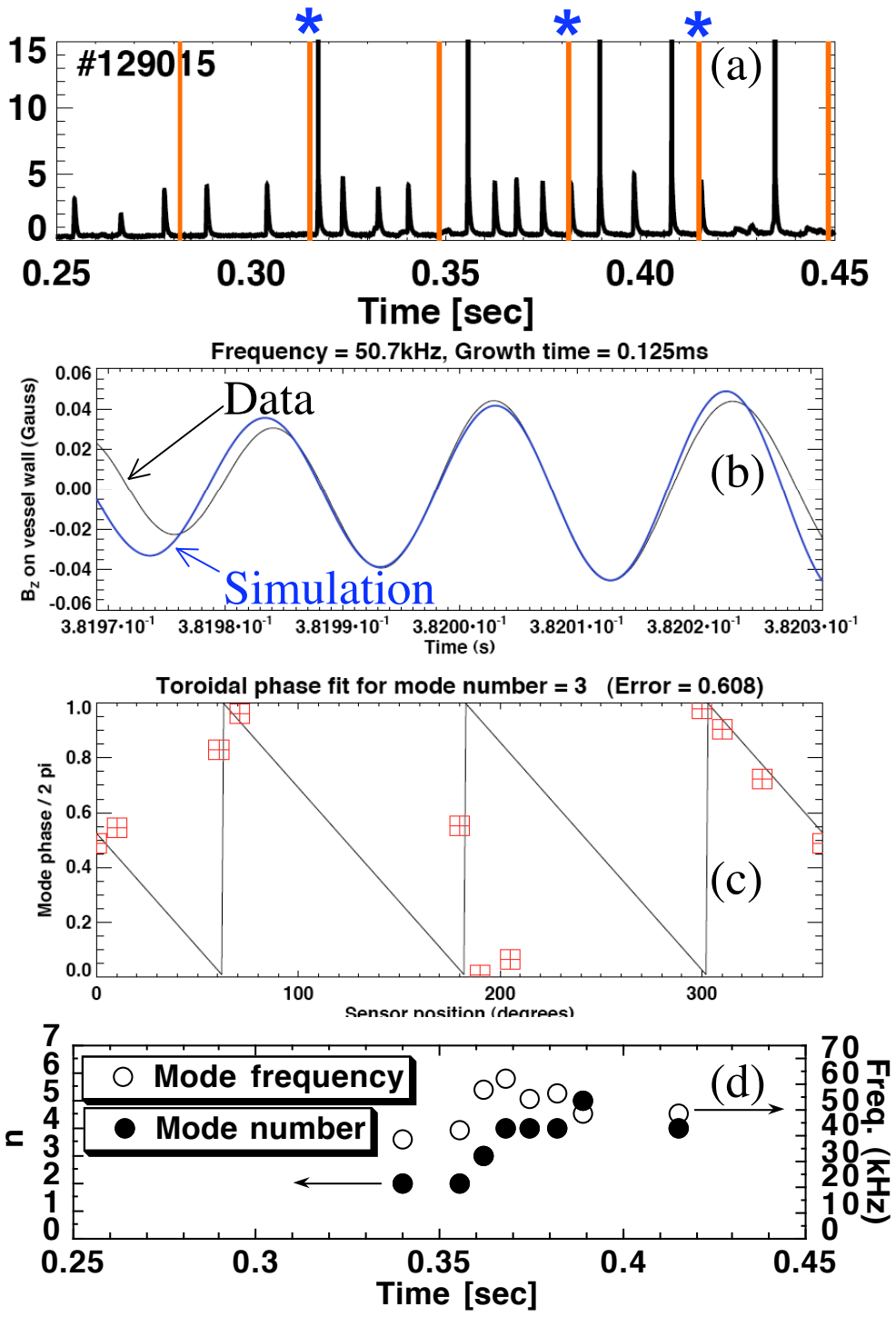
#129015
(a)
Time [sec]
Frequency = 50.7kHz, Growth time = 0.125ms
Data
Simulation
(b)
B_z on vessel wall (Gauss)
Time (s)
Toroidal phase fit for mode number = 3 (Error = 0.608)
Mode phase / 2 pi
(c)
Mode frequency
Mode number
(d)
n
Freq. (kHz)
Time [sec]

Figure 5

References

[1] F. Wagner, et. al., *Physical Review Letters* **49** (1982) 1408.

[2] H. Zohm, et. al., *Plasma Phys. Contr. Fusion* **38** (1996) 105.

[3] P. B. Snyder, H. R. Wilson, J. R. Ferron, L. L. Lao, A. W. Leonard, T. H. Osborne, A. D. Turnbull, D. Mossessian, M. Murakami, and X. Q. Xu, et. al., *Physics of Plasmas* **9** (2002) 2037.

[4] H. R. Wilson, P.B. Snyder, G.T.A. Huysmans, and R.L. Miller, et. al., *Physics of Plasmas* **9** (2002) 1277.

[5] C. M. Greenfield, K.H. Burrell, J.C. DeBoo, et. al., *Physical Review Letters* **86** (2001) 4544.

[6] T. E. Evans, R.A. Moyer, P.R. Thomas, et. al., *Physical Review Letters* **92** (2004) article #235003.

[7] R. Maingi, C.E. Bush, E.D. Fredrickson, et. al., *Nuclear Fusion* **45** (2005) 1066.

[8] M. Ono, S.M. Kaye, Y.-K.M. Peng, et. al., *Nuclear Fusion* **40** (2000) 557.

[9] A. R. Field, et. al., *Plasma Physics Controlled Fusion* **46** (2004) 981.

[10] R. Maingi, et. al., *Plasma Physics Controlled Fusion* **46** (2004) A305.

[11] V. A. Soukhanovskii, et. al., *Journal of Nuclear Materials* **313-316** (2003) 573.

[12] R. J. Akers, et. al., *Physical Review Letters* **88** (2002) 035002.

[13] M. A. Mahdavi, S.L. Allen, D.R. Baker, et. al., *J. Nucl. Materials* **220-222** (1995) 13.

[14] H. W. Kugel, M. Bell, D. Gates, et. al., *J. Nucl. Materials* **363-365** (2007) 791.

[15] H. W. Kugel, M. G. Bell, J.-W. Ahn, et. al., *Physics of Plasmas* **15** (2008) #056118.

[16] D. K. Mansfield, et. al., *J. Nucl. Materials* (2009) at press.

[17] H. W. Kugel, et. al., *J. Nucl. Mater.* (2009) at press.

[18] R. Kaita, H. Kugel, M.G. Bell, R. Bell, J. Boedo, et. al., *Proc. 22nd Fusion Energy Conference, Geneva, SZ, 13-18 Oct. 2008* (2008) paper EX/P4.

[19] S. F. Paul, et. al., *J. Nucl. Mater.* (2009) at press.

[20] J. M. Canik, R. Maingi, T.E. Evans, et. al., *Proc. 22nd Fusion Energy Conference, Geneva, SZ, 13-18 Oct. 2008.* (2008) paper PD/P1.

[21] S. M. Kaye, M. Greenwald, U. Stroth, et. al., *Nuclear Fusion* **37** (1997) 1303.

[22] T. H. Osborne, P.B. Snyder, K.H. Burrell, et. al., *J. Phys.: Conf. Series* **123** (2008) 012014.

[23] P. B. Snyder, K.H. Burrell, H.R. Wilson, M.S. Chu, M.E. Fenstermacher, et. al., *Nuclear Fusion* **47** (2007) 961.

[24] L. L. Lao, H. St. John, R.D. Stambaugh, A.G. Kellman, and W. Pfeiffer, et. al., *Nuclear Fusion* **25** (1985) 1611.

[25] O. Sauter, C. Angioni, and Y.R. Lin-Liu, et. al., *Physics of Plasmas* **6** (1999) 2834.

[26] R. Grimm, J. Greene, J. Johnson, et. al., *Methods Comput. Phys.* **16** (1976) 253.

[27] P. B. Snyder, H R Wilson, T H Osborne, and A W Leonard, et. al., *Plasma Physics Controlled Fusion* **46** (2004) A131.

[28] S. M. Kaye, J. Manickam, N. Asakura, et. al., *Nucl. Fusion* **12** (1990) 2621.

[29] S. A. Sabbagh, et. al., *Nuclear Fusion* **46** (2006) 635.